Article:

Hu, D, Guan, Z, Liu, M et al. (1 more author) (2022) Dynamical mechanisms for the recent ozone depletion in the Arctic stratosphere linked to North Pacific sea surface temperatures. Climate Dynamics, 58 (9-10). pp. 2663-2679. ISSN 0930-7575

https://doi.org/10.1007/s00382-021-06026-x

Dynamical Mechanisms for the Recent Ozone Depletion in the Arctic Stratosphere Linked to North Pacific Sea Surface Temperatures

Dingzhu Hu[1,*], Zhaoyong Guan[1,*], Meichen Liu[1], Wuhu Feng[2,3]

1. Key Laboratory of Meteorological Disasters of China Ministry of Education (KLME)/Joint International Research Laboratory of Climate and Environment Change (ILCEC)/Collaborative Innovation Center on Forecast and Evaluation of Meteorological Disasters (CIC-FEMD), Nanjing University of Information Science & Technology, Nanjing 210044, China

2. National Centre for Atmospheric Science, University of Leeds, Leeds, UK

3. School of Earth and Environment, University of Leeds, Leeds, UK

[*]To whom correspondence should be addressed.

E-mail: hudz@nuist.edu.cn; guanzy@nuist.edu.cn

Abstract

The stratospheric ozone layer, which prevents solar ultraviolet radiation from reaching the surface and thereby protects life on earth, is expected to recover from past depletion during this century due to the impact of the Montreal Protocol. However, how the ozone column over the Arctic will evolve over the next few decades is still under debate. In this study, we found that the ozone level in the Arctic stratosphere at 100–150 hPa during 1998–2018 exhibits a decreasing trend of -0.12 ± 0.07 ppmv decade^{-1} from MERRA2, suggesting a continued depletion during this century. About 30% of this ozone depletion is contributed by the second leading mode of sea surface temperature anomalies (SSTAs) over the North Pacific with one month leading and therefore is dynamical in origin. The North Pacific SSTAs associated with this mode tend to result in a weakened Aleutian low, a strengthened Western Pacific pattern and a weakened Pacific–North American pattern, which impede the upward propagation of wavenumber-1 waves into the lower stratosphere. The changes in the stratospheric wave activity may result in decreased ozone in the Arctic lower stratosphere through weakening the Brewer-Dobson circulation. Our findings uniquely linked the recent ozone depletion in the Arctic stratosphere to the North Pacific SSTs and might provide new understanding of how dynamical processes control Arctic stratospheric ozone.

1. Introduction

Stratospheric ozone, which comprises about 90% of the total amounts present in the Earth's atmosphere, is a radiatively and chemically active gas that shields the Earth from harmful solar ultraviolet radiation (WMO, 2018). In the stratosphere, ozone changes can alter the temperature and its gradient via radiative effects (Ramaswamy, 2001) and modify the circulation and wave activity via radiative–dynamical feedbacks (Hu & Tung, 2003; Eyring et al., 2007; Hu et al., 2015). Some studies have shown that depletion of stratospheric ozone during the austral summer may result in the poleward shift of the mid-latitude jet (e.g., Thompson et al., 2011; Son et al., 2018), widening of the Hadley circulation (Son et al., 2010), an increase in subtropical precipitation (Kang et al., 2011) and the poleward extension of the subtropical dry zones (Polvani et al., 2011) in the Southern Hemisphere. Ozone depletion over the Arctic may also affect sea-level pressure (SLP), temperature, and precipitation in most parts of the Northern Hemisphere (NH) (Calvo et al., 2015; Ivy et al., 2017), even the sea surface temperature anomalies (SSTAs) over tropical Pacific SSTs including El Niño–Southern Oscillation (ENSO) (Xie et al., 2017), though Harari et al. (2019) suggested that the Arctic stratospheric ozone may be not the proximate cause of the impacts on the surface over polar and tropical latitudes.

As the rapid increase in anthropogenic emissions of ozone depleting substances (ODSs) peaked in the mid-1990s (Weatherhead & Andersen, 2006), the globally averaged column ozone showed a negative trend from the late 1970s to the late 1990s

(WMO, 2007). With the observed decrease in ODSs in the atmosphere from the 1990s under the impact of the Montreal Protocol and its amendments (Chipperfield, 2015), numerical studies indicated that ozone concentrations in the upper stratosphere will recover due to the decreased ODSs (WMO, 2018). Chemistry–climate models predicted that ozone will recover to the levels of pre-1980 around 2050 (e.g., Weatherhead & Andersen, 2006). Bednarz et al. (2016) further reported that the ozone in the NH may recover to 1980 levels by about 2030–2040. Results from Chemistry-Climate Model Initiative (CCMI) simulations project under a Representative Concentration Pathway (RCP) of 6.0 showed that the column ozone will return to 1980 values in 2032 (2020–2044) at mid-latitudes but in 2034 (2025–2043) at high-latitudes in the NH (Dhomse et al., 2018).

Datasets from National Aeronautics and Space Administration (NASA) and National Oceanic and Atmospheric Administration (NOAA) satellites show that ozone in the mid- and upper stratosphere increased slowly during 2000–2016 (Steinbrech et al., 2017). However, some studies have suggested that there was no significant trend in the ozone levels in the lower stratosphere from 1984 to 2011 (Tummon et al., 2015) or from 1995 to 2013 (Cohen et al., 2018). Some other studies reported that the ozone concentrations derived from merged datasets in the lower stratosphere between 40°S–40°N after 1997 (Bourassa et al., 2014) and between 60°S–60°N after 1998 (e.g., Ball et al., 2018, 2020; Wargan et al., 2018) were still decreasing. Given the declining ODS concentrations, extensive research, vigorous debate and a number of papers tried to refine the results and propose potential mechanisms after the continuing decline of the lower stratospheric ozone in the 21st century was first found by Ball et al. (2018). While these above-mentioned studies focused on tropical and midlatitudinal ozone trends, the result on the ozone over the Arctic is still unclear. Note that there has been a significant chemical depletion of ozone during some Arctic cold stratospheric winters during the past two decades (Tilmes et al., 2004; Manney et al., 2015). For example, the magnitude of the reduction in ozone concentrations over the Arctic observed during the late winter and early spring in 2011 was comparable with that over the Antarctic (e.g., Manney et al., 2011; Hurwitz et al., 2011). The lowest observed ozone levels in the Arctic occurred in 2020, which covered an area about three times the size of Greenland (e.g., Witze, 2020; Dameris et al., 2020; Innes et al., 2020; Lawrence et al., 2020; Manney et al., 2020; Wohltmann et al., 2020; Xia et al., 2021). The above mentioned numerical and observational results point to two elements: the apparent negative trends over the past two decades constitute a new and intriguing result and large variability is a confounding factor in trend estimation.

Stratospheric ozone is not only affected by chemical processes related to ODSs (Rex et al., 2004), but is also modulated by SSTs via dynamical processes (e.g., Hu et al., 2014). Some studies suggested that SSTs in the North Pacific have significant impacts on the stratospheric Arctic vortex (e.g., Hurwitz et al., 2012; Hu et al., 2018). Hu et al. (2018) reported that the warming over the central North Pacific may lead to a strengthening of the stratospheric vortex over the Arctic during the boreal winter. Other studies revealed that the Arctic vortex in the stratosphere is related to the concentrations of ozone there (e.g., Hu et al., 2015). Polar vortices in cold years would have increased polar stratospheric clouds (PSCs) occurrence, on the surface of which chlorine-activating heterogeneous reactions occur, further reducing the ozone (Solomon et al., 1994; Chipperfield et al., 1999; Daniel et al., 1999). Strength of the polar vortex during boreal winter is partly controlled by wave driving (e.g., Newman et al., 2001; Hu et al., 2018). The stronger and more variable wave driving can affect the ozone concentrations by both ozone transport (i.e., dynamical resupply) and chemical depletion (e.g., Strahan et al., 2016), i.e., stronger (weaker) wave driving is closely associated with increased (decreased) ozone by dynamical resupply and increased (decreased) ozone by reducing (increasing) ozone loss. A question therefore arises about whether the ozone concentrations in the stratosphere over the Arctic are affected by the SSTs over the North Pacific and how can these SSTs affect stratospheric ozone.

To answer the above questions, the reanalysis, observational datasets and a chemical transport model (CTM) are used to investigate the trends in ozone concentrations over the Arctic in the lower stratosphere during 1998–2018 and provide a dynamical mechanism. Our results show that the ozone has declined during this period, which can be ascribed to the second leading mode of the SSTAs over the North Pacific or the Victoria mode, the low-frequency variability in the SSTAs over the North Pacific that cannot be explained by the Pacific decadal oscillation alone (Bond et al., 2003; Ding et al., 2015). The SSTAs over the North Pacific associated with the Victoria mode influence stratospheric ozone through reducing the upward propagation of the wavenumber-1 wave in the extratropical stratosphere, weakening the Brewer-Dobson circulation (BDC). The recent depletion of ozone in the Arctic lower stratosphere and its links to the North Pacific SSTs suggest that some potential dynamical processes play a key role in the stratospheric ozone variations over the Arctic, not only the ODSs controlled by the Montreal Protocol and the associated chemical processes. It is worth clarifying that a trend of two decades could reflect decadal variability that is likely to reverse going forward.

2. Data, numerical experiments and methods

2.1 Datasets

The monthly mean datasets of temperature, winds, geopotential height, SLP, and ozone during 1980–2018 from Modern-Era Retrospective Analysis for Research and Applications version 2 (MERRA2) (Gelaro et al. 2017) are used in this study. Because the observations assimilated in reanalysis over the course of many decades are highly non-homogeneous, changes in input data can and do lead to significant discontinuities in all assimilated fields (e.g., Davis et al., 2017; Wargan et al. 2018). Following the method in Wargan et al. (2018), we have removed the discontinuities of MERRA2 reanalysis by step changes using the results from the reference run in TOMCAT/SLIMCAT (hereafter TOMCAT, described in section 2.2) (Chipperfield et al., 2006) as a transfer function standard. And the results suggested that the discontinuities of MERRA2 are not an issue in the regions of 65°–90°N and 100–150 hPa we focused on (figure not shown). Wargan et al. (2018) have demonstrated that the ozone record from MERRA2 can be homogenized allowing reliable trend calculations.

We also used the monthly mean ozone datasets from European Centre for Medium-Range Weather Forecasts fifth generation atmospheric reanalyses (ERA5)

(Hersbach et al. 2019), Global OZone Chemistry And Related trace gas Data records for the Stratosphere (GOZCARDS) (Froidevaux et al. 2015), partial column ozone field from Solar Backscattered Ultraviolet (SBUV) (Kramarova et al. 2013; Bhartia et al. 2013), Stratospheric Water and OzOne Satellite Homogenized (SWOOSH) (Davis et al. 2016), Microwave Limb Sounder (MLS) (Schwartz et al. 2021). The SST data from the Extended Reconstructed Sea Surface Temperature V5 (Huang et al. 2017) was used. The description of above data sources is listed in Table 1.

Table 1. Description of the data sources used in this work.

Datasets	Download websites	References
MERRA2	https://disc.gsfc.nasa.gov/datasets/M2IMNPASM_V5.12.4/summary?keywords=merra-2	Gelaro et al. (2017)
ERA5	https://cds.climate.copernicus.eu/cdsapp#!/dataset/reanalysis-era5-pressure-levels-monthly-means?tab=form	Hersbach et al. (2019)
GOZCARDS	https://disc.gsfc.nasa.gov/datasets/GozSmlpO3_V1	Froidevaux et al. (2015)
SBUV	https://disc.gsfc.nasa.gov/datasets/SBUV2N09L3zm_V1	Kramarova et al. (2013); Bhartia et al. (2013)
SWOOSH	http://www.esrl.noaa.gov/csd/groups/csd8/swoosh/	Davis et al. (2016)
MLS	https://disc.gsfc.nasa.gov/datasets/ML3MBO3_005/summary?keywords=MLS	Schwartz et al. (2021)
ERSST V5	https://www.esrl.noaa.gov/psd/data/gridded/data.noaa.ersst.v5.html	Huang et al. (2017)

2.2 Model and simulations

We also used a three dimensional (3D) chemical transport model TOMCAT/SLIMCAT (hereafter TOMCAT) (Chipperfield, 2006). This model has a good description of chemistry for both the troposphere and stratosphere, which include the heterogeneous reactions on sulfate aerosols and liquid/solid polar stratospheric clouds (Chipperfield et al., 2018a) as well as chemistry reactions of the oxygen, nitrogen, hydrogen, chlorine and bromine families (Grooss et al., 2018). More details about TOMCAT can be found in Chipperfield et al. (2018a).

Two experiments have been designed. Both simulations were forced by the temperature and winds fields from European Centre for Medium-Range Weather Forecasts ERA-Interim reanalysis (Dee et al., 2011). The model has a horizontal resolution of 2.8° × 2.8° and the vertical levels from the surface up to ~60 km (Chipperfield, 2006). The only difference between the reference run and sensitivity run (ODSfix) (Feng et al., 2021) is that the ODSs after year 1995 are fixed in the sensitivity run but are time-varying in the reference run. The ODSs in the experiments are obtained from WMO (2018).

2.3 Methods

As the BDC is a Lagrangian mean circulation, approximated by the residual mean meridional circulation of the transformed Eulerian-mean equations (Dunkerton 1978), the various processes that can influence the ozone could be separated into the ozone advection by the BDC or mean ozone transport, the large-scale eddy transport, and the chemical net production term (Garcia and Solomon, 1983). The zonal mean ozone tracer continuity equation in the transformed Eulerian-mean formulation in spherical geometry following Garcia and Solomon (1983), is as follows:

$$\frac{\partial \bar{\chi}}{\partial t} = -\frac{\bar{v}^*}{a}\frac{\partial \bar{\chi}}{\partial \varphi} - \bar{w}^*\frac{\partial \bar{\chi}}{\partial z} - \frac{1}{\rho_0}\nabla \cdot \boldsymbol{M} + \bar{S} \tag{1}$$

$$\bar{v}^* = \bar{v} - \frac{1}{\rho_0}\frac{\partial}{\partial z}\left(\rho_0 \frac{\overline{v'\theta'}}{\overline{\theta_z}}\right) \ ; \quad \bar{w}^* = \bar{w} + \frac{1}{a\cos\varphi}\frac{\partial}{\partial \varphi}\left(cos\varphi \frac{\overline{v'\theta'}}{\overline{\theta_z}}\right) \tag{2}$$

$$\boldsymbol{M}^{(\varphi)} = \rho_0\left(\overline{v'\chi'} - \frac{\overline{v'\theta'}}{\overline{\theta_z}}\frac{\partial \bar{\chi}}{\partial z}\right) \ ; \ \boldsymbol{M}^{(z)} = \rho_0\left(\overline{\omega'\chi'} + \frac{1}{a}\frac{\overline{v'\theta'}}{\overline{\theta_z}}\frac{\partial \bar{\chi}}{\partial \varphi}\right) \tag{3}$$

where $\bar{\chi}$ is the zonal mean ozone concentration, $\bar{v}^*$ and $\bar{w}^*$ calculated as Eq. (2) are the BDC's meridional and vertical velocities, respectively, defined by Andrews et al.

(1987). $\bar{S}$ is the chemical net production of ozone. The variables v and w are the meridional and vertical winds, respectively, θ is the potential temperature, a is the Earth's radius, ρ_0 is air density, t, φ and z are time, latitude, and height, respectively. The overbars represent the zonal mean and the primes denote the departure from the zonal mean. The first and second terms on the right-hand side of Eq. (1) represent the advection of ozone by the BDC and the mean ozone transport. The eddy flux $\boldsymbol{M}$ is defined in Eq. (3) by Garcia and Solomon (1983) and represents the ozone flux related to the eddies caused by the wave component. $\nabla \cdot \boldsymbol{M}$ is the eddy flux ($\boldsymbol{M}$) divergence. So the third term in Eq. (1) represents the ozone caused by the large-scale eddy transport. The fourth term $\bar{S}$ in Eq. (1) represents the chemical net production of ozone.

The linear trends and their statistical significance were estimated with the Sen median slope (Sen 1968) and the Mann–Kendall (Kendall 1975) method, respectively, since the nonparametric methods are less sensitive to outliers. In addition, the two-tailed Student's *t* test is used to test the statistical significance of the regression and correlation coefficients between two auto-correlated time series. The effective number of degrees of freedom N^{eff} is expressed below as Pyper and Peterman (1998):

$$\frac{1}{N^{eff}} = \frac{1}{N} + \frac{2}{N}\sum_{j=1}^{N} \frac{N-j}{N} \rho_{XX}(j)\rho_{YY}(j) \qquad (4)$$

where N is the sample size and $\rho_{XX}(j)$ and $\rho_{YY}(j)$ are the auto-correlations of the two sampled time series X and Y at time lag j, respectively.

3. Decreasing trend in the ozone over the Arctic in the lower stratosphere

Ivy et al. (2017) suggested that changes in the stratospheric ozone in March is a useful indicator for the climate anomalies in the troposphere in the NH. Xie et al. (2017) further revealed that changes in the stratospheric ozone over the Arctic has strongest linkage between the SSTs over the North Pacific in April. These previous studies suggested the importance of the stratospheric ozone over the Arctic in March. Figure 1 displays the trends in the zonal mean ozone concentrations in March derived from MERRA2 reanalysis and reference simulation in TOMCAT during 1998–2018. Downward trends in the March zonal mean ozone mixing ratios are observed in the lower stratosphere over the Arctic during the period 1998–2018 in MERRA2 (Fig. 1a), ERA5 (Fig. 1b), and TOMCAT (Chipperfield, 2006) (Fig. 1c), with the largest negative trends occurring in the subpolar regions 50°–70°N at 100–150 hPa. The negative trends during 1998–2018 from MERRA2 and ERA5 can also be observed during different periods with the start year shifted several points earlier or later (figure not shown). Therefore, the negative ozone trend in the lower stratosphere (100-150 hPa) over the Arctic is not much influenced by the samples in some unusual years and is persistent during 1998–2018. The time series of ozone averaged over 65°–90°N from 100–150 hPa (hereafter O_{3_ALS}) during 1998–2018 (Fig. 1d) also shows statistically significant negative trends of –0.12±0.07 ppmv decade^{-1} from MERRA2 and –0.07±0.06 ppmv decade^{-1} from TOMCAT, respectively. Also, the year-to-year variability of ozone in the lower stratosphere over the Arctic from MERRA2 and TOMCAT (Fig. 1d) can be observed clearly and is highly consistent, with a correlation coefficient *r* equals to 0.87, significant above the 95% confidence level. Moreover, the levels of ozone from

MERRA2 are highly correlated with those from SWOOSH (r = 0.91), GOZCARDS (r = 0.82), and SBUV (r = 0.92) with these three correlation coefficients all significant above the 95% confidence level. These results suggest that the downward trend of ozone in the stratosphere over the Arctic is reliable. Note that the pattern of the negative trend in ozone from MERRA2 during 1998–2018 excluding 2011 (figure not shown) is similar to that includes 2011 (Fig. 1a). Trends in O_{3_ALS} during 1998–2018 excluding 2011 is –0.11±0.07 ppmv decade^{-1}, which is slightly smaller than the results including 2011. This implies that the year 2011 makes a contribution to the negative trend in ozone during 1998–2018, but the downward trend in Arctic ozone in the stratosphere during this period is not dominated by the large 2011 Arctic winter/spring ozone loss event.

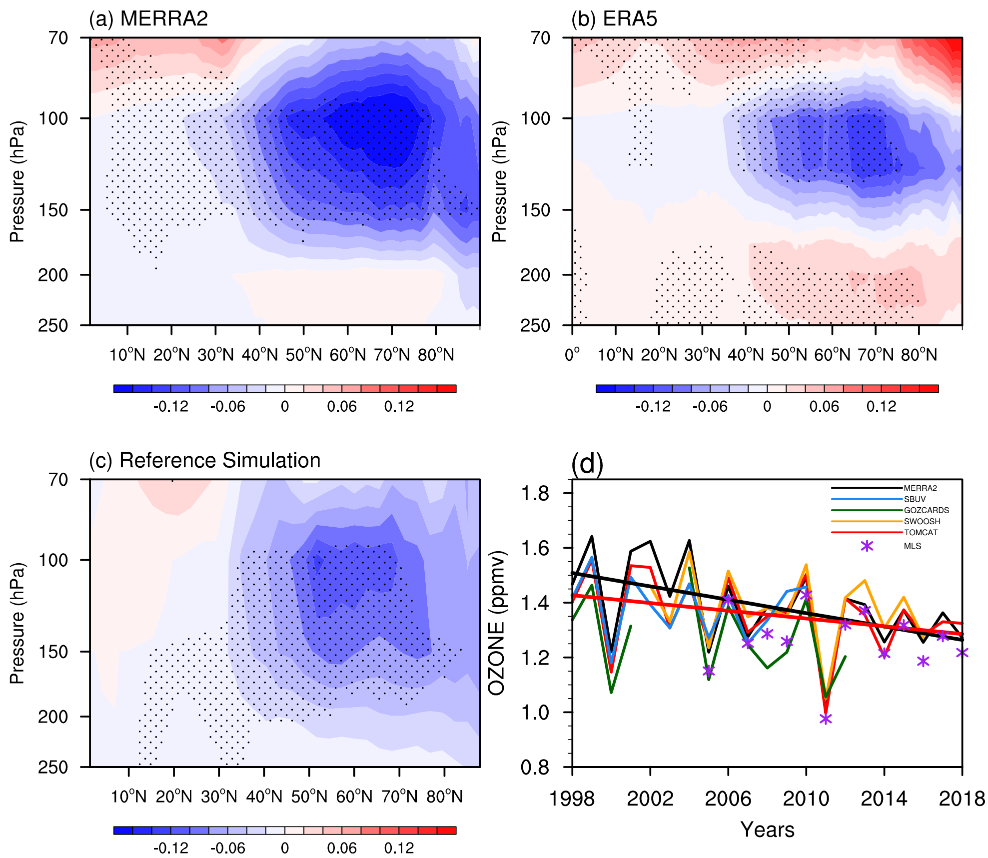

Figure 1. (a–c) Trends (units: ppmv decade^{-1}) in the zonal mean ozone concentrations

in March derived from the (a) MERRA2 reanalysis, (b) ERA5 reanalysis, and (c) reference simulation from TOMCAT during 1998–2018. Stippled regions represent the values significant at/above the 90% confidence level. (d) Time series of ozone concentrations averaged over 65°–90°N and 100–150 hPa derived from different databases in March. The black and red straight lines represent the linear trends of ozone concentrations from MERRA2 and reference run in TOMCAT, respectively.

Note that the negative trends in the lower stratospheric ozone over the Arctic from MERRA2 and TOMCAT are also observed during the period 1980–1997, which is shown in Fig. 2. The statistically significant decreasing ozone trends at high-latitude before 1980–1997 indicate a depletion of Arctic stratospheric ozone, consistent with previous studies (WMO, 2018). However, the negative ozone trends at high-latitude in the lower stratosphere during 1980–1997 (Fig. 2) are larger than those during 1998–2018 (Fig. 1), which is possibly because of the decreased ODSs during the latter period (WMO, 2018). Previous studies revealed that the concentration of stratospheric ozone from 1979 to mid-1990s exhibits a significant decreasing trend, and it is expected to recover to the level of pre-1980 around the middle of this century under the impacts of Montreal Protocol and its Amendments (e.g., Weatherhead & Andersen, 2006; WMO, 2018). However, the observations and simulation (Fig. 1) presented here all show a continued decreasing trend in the levels of ozone in the lower stratosphere over the Arctic after the 2000s, which suggests that the levels of ozone in this region have not started to recover as expected, but the downward trend after the 2000s is slightly smaller because of the deceasing ODS levels. This is consistent with the results in Garfinkel et al. (2015).

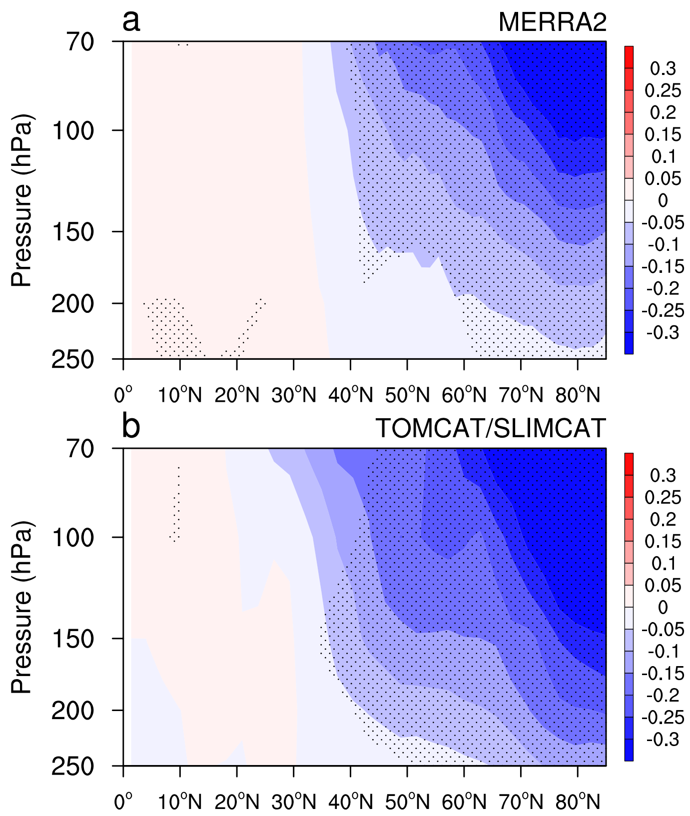

Figure 2. Trends (units: ppmv decade^{-1}) in the ozone concentrations during 1980–1997 in March from (a) MERRA2 and (b) TOMCAT. Stippled areas represent the values at/above 95% level of confidence.

To further verify the role of ODSs played in the ozone trends after the 2000s, the sensitivity experiment in which ODSs are fixed after the 1995 has been designed. More details are provided in Section 2.2. Figure 3 gives the trends in the zonal mean ozone concentrations in March from reference run and ODSfix run in TOMCAT during 1998–2018. The trends in ozone concentration in the stratosphere over the Arctic in two simulations are both statistically significantly negative, with smaller negative trends in reference run (Fig. 3a) but larger negative trends in ozone in ODSfix run (Fig. 3b). This smaller negative trend in ozone between the sensitivity and reference simulations in

TOMCAT (Fig. 3) not only confirms the role of decreased ODSs after mid 1990s, but also suggests that some other processes might also influence the trends in ozone over the Arctic in the stratosphere.

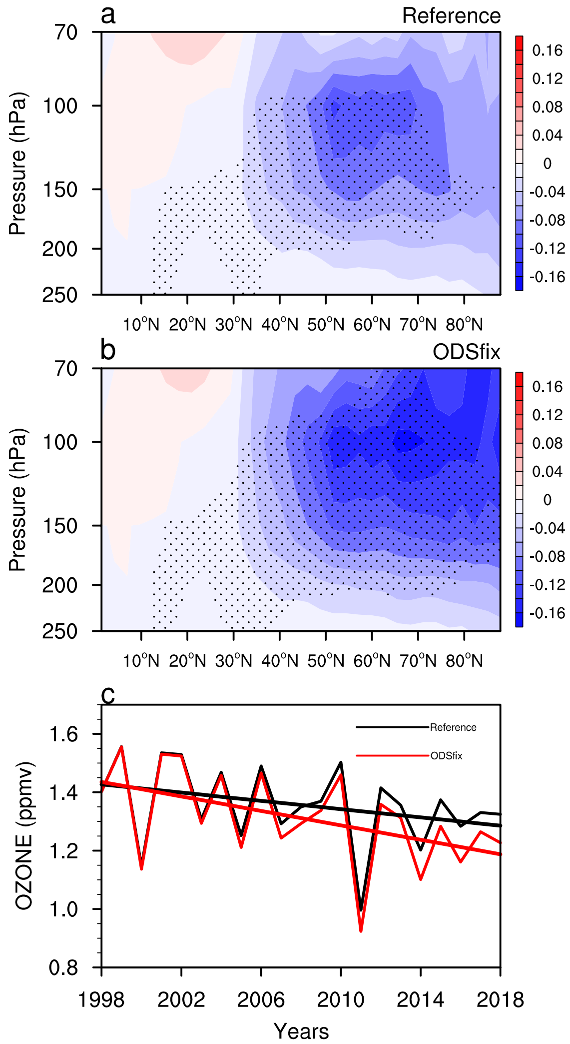

Figure 3. Trends (units: ppmv decade^{-1}) in the zonal mean ozone concentrations in March derived from TOMCAT during 1998–2018, (a) reference run and (b) ODSfix run. Stippled regions represent the values statistically significant at/above the 90% confidence level. (c) Time series of O_{3_ALS} from two simulations in March. The black and red straight lines represent the linear trends of ozone concentrations from reference and sensitivity runs, respectively.

4. Connections between the Arctic ozone and North Pacific SSTAs

The factors that affect the stratospheric ozone concentrations include the ODSs through chemical reactions (e.g., Rex et al., 2004) and the SSTs via dynamical processes (e.g., García-Herrera et al., 2006; Manzini et al., 2006; Hu et al., 2014). Previous studies suggested the delayed impacts of tropical SSTs on the stratosphere (e.g., García-Herrera et al., 2006; Manzini et al., 2006) and a significant impact of the North Pacific SSTAs on the stratospheric polar vortex (e.g., Hurwitz et al., 2012; Hu et al., 2018). However, the connection between the lower stratospheric ozone over the Arctic and the SSTAs over the North Pacific is still unclear. Figure 4 shows the regressed SSTAs over the North Pacific in February based on the normalized O_{3_ALS} index during 1980–2018 in March. From Fig. 4a, the SSTAs exhibit a northeast-southwest-oriented dipole pattern, i.e., the band of positive anomalous values that extends from the coast of California across the Pacific to the western Bering Sea, and the band of negative anomalous values from the central North Pacific to the coast of Asia. This pattern resembles the spatial pattern of the second leading mode of the SSTAs over the North Pacific (Bond et al., 2003; Ding et al., 2015). Following Bond et al. (2003), we adopted the monthly North Pacific (100° E–100.5° W, 20.5–65.5° N) SSTAs during 1980–2018 in February to perform an Empirical Orthogonal Function (EOF) reanalysis. Its second EOF mode (EOF2) (Fig. 4b) resembles the pattern of the second leading mode of the North Pacific SSTAs or Victoria mode (Bond et al., 2003; Ding et al., 2015), accounting for 18.7% of the total variance. As expected, the pattern of the regressed SSTAs over the North Pacific in February based on the normalized O_{3_ALS} index in March (Fig. 4a) is similar to that of the EOF2 of North Pacific SSTAs (Fig. 4b), appearing as a Victoria-like mode. This suggests that ozone levels over the Arctic in the lower stratosphere in March are possibly related to the SSTAs over the North Pacific associated with the Victoria mode in February. It would be interesting to understand the role of ENSO, because of its impacts on the stratospheric polar vortex (e.g., Sassi et al. 2004; Manzini et al., 2006; Garfinkel and Hartmann 2008; Xie et al., 2012; 2014; Rao and Ren 2016). However, there are no significant trends in the Multivariate ENSO Index index from 1998 to 2018 in March and the SSTAs related to the stratospheric ozone over the Arctic are statistically insignificant over the tropical Pacific Ocean (figure not shown). It implies that ENSO might be not a dominant role in modulating the trends in the stratospheric ozone over the Arctic after 1998.

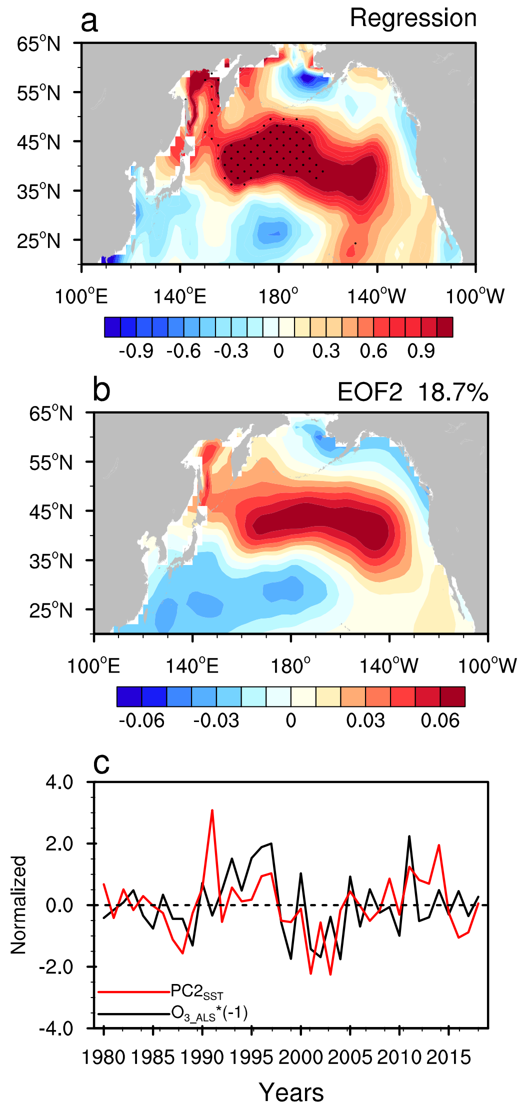

Figure 4. (a) Regression of SSTAs (unit: K) over the North Pacific in February on the normalized O_{3_ALS} index in March during 1980–2018. The dotted values are significant at/above the 90% confidence level. (b) EOF2 of the North Pacific SSTAs (20.5–65.5°N, 100°E–100.5°W) in February during 1980–2018. The top-right value is the explained variations of EOF2. Time series of the normalized $PC2_{SST}$ (red line) and O_{3_ALS}×(–1) (black line) is shown in (c).

To verify the impacts of the SSTAs over the North Pacific associated with the Victoria mode on the ozone over the Arctic in the stratosphere in March, we also calculated the correlations between the normalized O_{3_ALS} index in March and the second principal component ($PC2_{SST}$) of North Pacific SSTAs in October–March that leads the O_{3_ALS} by 5 to 0 months, shown in Table 2. The results show that the highest and statistically significant correlation of $PC2_{SST}$ with O_{3_ALS} in March occurs in February ($PC2_{SST}$ leads O_{3_ALS} by one-month), suggesting that changes in the SSTAs over North Pacific associated with the Victoria mode in February may influence ozone in the Arctic lower stratosphere.

Table 2. Correlations of O_{3_ALS} in March during 1998–2018 with $PC2_{SST}$ in October, November and December during 1997–2017, January, February, and March during 1998–2018, respectively. $PC2_{SST}$ leads O_{3_ALS} in March during 1998–2018 by 5 to 0 months. Values with asterisks are for those at/above 95% confidence level.

Correlations	October	November	December	January	February	March
O_{3_ALS}	–0.08	–0.01	0.19	0.38	0.46*	0.35

An in-phase relationship between the $PC2_{SST}$ in February and O_{3_ALS}×(–1) (here the negative O_{3_ALS} is used for purposes of visualization) (Fig. 4c) can clearly be seen, and the correlation coefficient between $PC2_{SST}$ and O_{3_ALS} is –0.40 during 1980–2018 and –0.47 during 1998–2018, respectively, with both values significant at/above the 95% confidence level. Note that the correlation coefficient between these two indices is only –0.27 during 1980–1997, which is insignificant at the 90% confidence level. Similar results can be seen in TOMCAT data (figure not shown). This implies that there is an out-of-phase linkage between the lower-stratospheric ozone over the

Arctic and SSTAs associated with the Victoria mode, but that this out-of-phase relationship is much stronger during 1998–2018. The interannual correlation between lower-stratospheric ozone over the Arctic and North Pacific SSTAs suggests that the decreasing Arctic lower stratospheric ozone trends during 1998–2018 (Fig. 1) are connected to the trends in the North Pacific SSTAs associated with the Victoria mode. The linear trend in $PC2_{SST}$ during 1998–2018 in February is consistent with the trend in O_{3_ALS}×(−1) during 1998–2018 in March (Fig. 4c).

To quantify the contributions from different factors to ozone trends in the Arctic lower stratosphere, a multiple linear regression (MLR) was considered as follows:

$$Ozone(\varphi, p, t) = \sum_{i=1}^{8} \alpha_i \, (\varphi, p) \cdot F_i(t) + residual$$

Where $Ozone(\varphi, p, t)$ is the interannual variability of zonal mean ozone concentration in March. Here the interannual variability of one variable is obtained by subjecting it to a seven-year high-pass Lanczos filter (Duchon 1979). φ, p, and t represent the latitude, level, and time, respectively. Variables F_1, F_2, F_3, F_4, F_5, F_6, F_7 and F_8 denote the interannual variabilities of stratospheric aerosol depth at 550 nm (SAD; the SAD before 1990 is downloaded from https://data.giss.nasa.gov/modelforce/strataer/tau.line_2012.12.txt and after 1990 is from http://dx.doi.org/10.5065/D6S180JM), NPSST (represented by the $PC2_{SST}$ index), multivariate ENSO index (NINO) (https://www.esrl.noaa.gov/psd/data/correlation/nina34.data), quasi-biennial oscillation (QBO) index at 30 hPa (https://www.esrl.noaa.gov/psd/data/correlation/qbo.data), solar cycle (SC, represented by the 10.7 cm solar flux; https://www.esrl.noaa.gov/psd/data/correlation/solar.data), sea ice concentration (SIC) from HadISST data (http://hadobs.metoffice.com/hadisst/data/download.html), CO_2 concentration (from the IPCC AR4 B1 scenarios, IPCC, 2007), and the tripole-like SSTAs over the North Atlantic (NASST), respectively. Some studies revealed that the North Atlantic also plays a role in the stratospheric Arctic vortex (e.g., Garfinkel et al., 2015; Hu et al., 2019). Figure 5 displays the trends in the SSTAs over the North Atlantic during 1998–2018. The trends in the North Atlantic SSTAs during this period exhibit a tripole-like pattern, with significant positive anomalies in the subtropical western North Atlantic and negative values in the tropical and subpolar eastern North Atlantic, which resembles the SSTAs in previous studies (e.g., Rodwell et al., 1999; Sutton et al., 2000; Czaja and Marshall, 2001; Peng et al., 2003). Therefore, a NASST index is defined as the SSTAs averaged over a southern box (35°–45°N, 50°W–70°W) minus that in a northern box (50°–60°N, 20°W–40°W) according to Fig. 5.

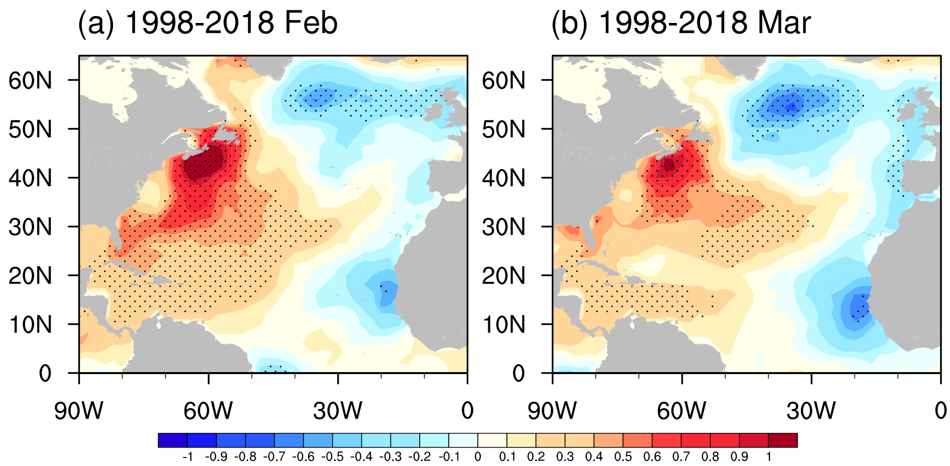

Figure 5. Trends in the SSTAs (unit: K/decade) from ERSST V5 in (a) February and (b) March during 1998–2018. The values over the stippled regions are statistically significant at/above the 95% confidence level.

The trends in the ozone concentrations contributed from different factors are estimated by the linear trends of $\alpha_i(\varphi, p) \cdot Trend_{F_i}/Trend_{ozone}$ ($i = 1, 2, 3, 4, 5,6,7,8$). As we focused on the trends in the ozone averaged over 65°–90°N from 100–150 hPa during 1998–2018, the contributions of different factors to the lower stratospheric ozone over the Arctic are calculated by the coefficient $\alpha_i(\varphi, p)$ averaged over 65°–90°N from 100–150 hPa multiplied by the trends in different factors over ozone during 1998–2018. Figure 6 shows the contributions of the various factors including solar cycle, QBO, ENSO, North Pacific SSTAs, CO_2, sea ice, stratospheric aerosol, and North Atlantic SSTAs to the recent decreasing trend in ozone. A key point here is that the North Pacific SSTAs associated with Victoria mode is the largest contributor to the decreased ozone over the lower stratospheric Arctic after the 2000s, which contributes ~30% to the decreased trend in the lower stratospheric ozone over the Arctic.

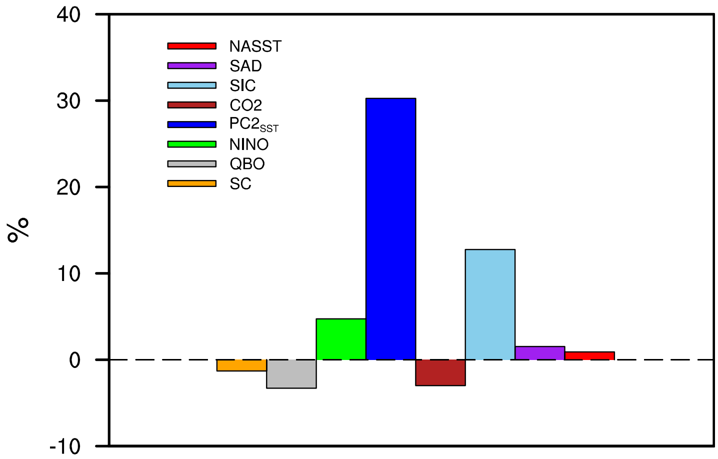

Figure 6. Contributions (%) from different factors (NASST, SAD, SIC, CO2, North Pacific SSTs, ENSO, QBO and SC) using the MLR equation to O_{3_ALS} during 1998–2016.

5. Dynamic mechanisms

We will now provide evidence for a causal mechanism linking the SSTAs associated with the Victoria mode to the concentrations of lower-stratospheric ozone over the Arctic. The variability of the ozone in the upper stratosphere were shown to be dominated by chemical processes, while ozone in the lower stratosphere is strongly affected by dynamical processes (e.g., Douglass et al., 1985; Hartmann et al., 1981; Wargan et al., 2018; Ball et al., 2020; Orbe et al., 2020). And the SSTAs over the North Pacific were suggested to have significant effects on the stratospheric Arctic vortex via dynamical processes (e.g., Hurwitz et al., 2012; Hu et al., 2018). Therefore, it is worthwhile to investigate the possible dynamical mechanisms affecting ozone concentrations in the lower stratosphere over the Arctic in response to the North Pacific SSTAs.

Figure 7 gives the trends in the geopotential height and horizontal winds at 200 and 500 hPa in March during 1998–2018. The geopotential height at both 200 and 500 hPa exhibits statistically significant positive trends north of 35°N in the North Pacific, along with anticyclonic trends in the horizonal winds (Figs. 7a–b). The regressed anomalies in the geopotential height and horizontal winds at 200 and 500 hPa in March from MERRA2 based on the $PC2_{SST}$ in February during 1980–2018 (Figs. 7c–d) are similar to the pattern of tropospheric circulation trends during 1998–2018 (Figs. 7a–b), but the magnitudes of the anomalies in the geopotential height and horizontal winds related to the North Pacific SSTAs are smaller than those of the trends. In response to the second leading mode of North Pacific SSTAs, there are statistically significant positive anomalies in the geopotential height at 200 hPa occurring in the north of 35°N in the North Pacific, accompanied by anticyclonic anomalies in the horizontal winds (Fig. 7c). The $PC2_{SST}$-related geopotential height over the southwestern North Pacific exhibits negative anomalies accompanied with cyclonic horizontal wind anomalies. The pattern of geopotential height over the North Pacific is consistent with that at 500 hPa (Fig. 7d), also similar to that of SST (Fig. 4b), which indicates a weakened Aleutian low in response to $PC2_{SST}$. A previous study has revealed that the warming in the central North Pacific corresponds to a weakened Aleutian low (Hu et al., 2018), consistent with our result here. Tropospheric teleconnection patterns, such as the Western Pacific (WP) and Pacific–North American (PNA) patterns, can be characterized by a deep Aleutian low (Wallance & Gutzler, 1981). The correlation coefficients between the $PC2_{SST}$ and WP, PNA teleconnection patterns at 200 hPa following the definitions in Wallace and Gutzler (1981) are 0.43 and –0.37, respectively, both above the 95% confidence level. This implies that in response to the positive Victoria mode, the WP teleconnection pattern strengthens but the PNA teleconnection pattern weakens.

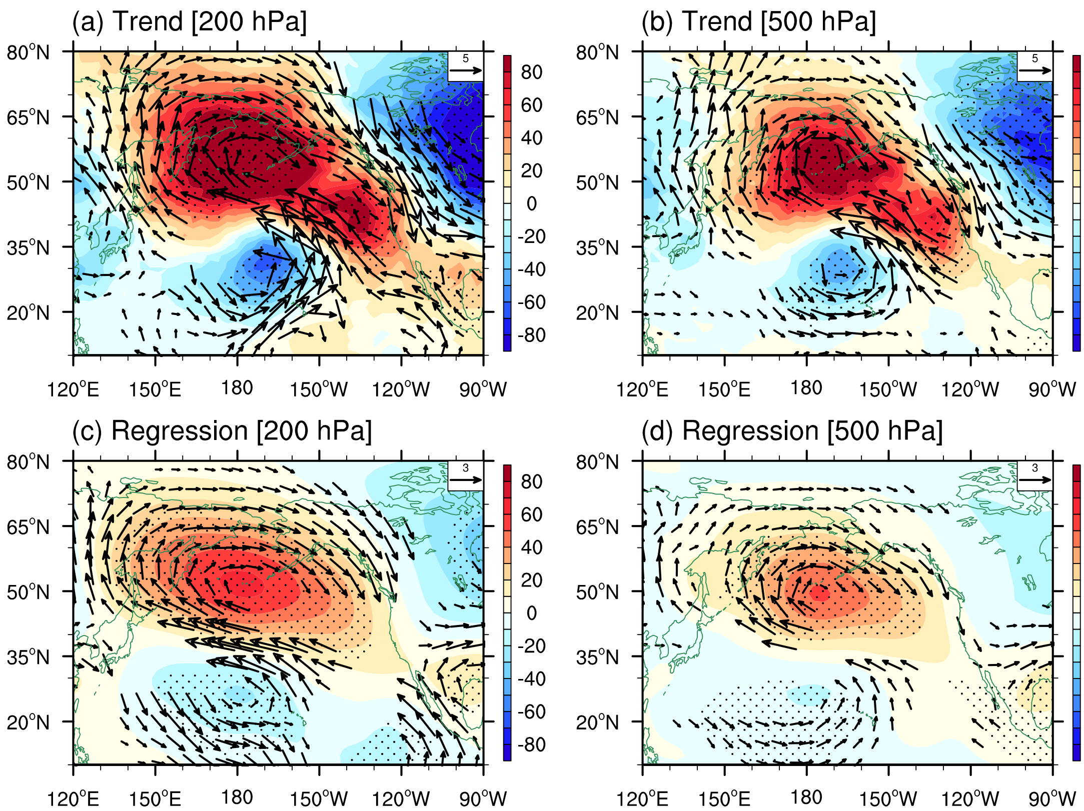

Figure 7. (a, b) Trends in the geopotential height (shading, m decade^{-1}) and horizontal winds (vectors, only values above 0.5 m s^{-1} decade^{-1} are shown) at (a) 200 hPa and (b) 500 hPa in March during 1998–2018. (c, d) Same as (a, b), but for the anomalies in the geopotential height (shading) and horizontal winds (vectors, only values above 0.5 m s^{-1} are shown) at (a) 200 hPa and (b) 500 hPa in March obtained by the regression of the $PC2_{SST}$ in February during 1980–2018. Dotted regions represent the values statistically significant at the 90% confidence level.

The weakened Aleutian low, accompanied by the strengthened WP and weakened PNA patterns, may affect the wave activity in the stratosphere (Hu et al., 2018). Therefore, trends in the longitudinal and vertical structures of the wavenumber-1 and -2 components of geopotential height averaged over 45°N–75°N during 1998–2018 are shown in Figs. 8a–b. Trends in the zonal wavenumber-1 component are out-of-phase with its climatologies, i.e., the positive (negative) trends are co-located with the negative (positive) climatologies (Fig. 8a). Whereas the trends in the wavenumber-2 component are in-phase with its climatologies, exhibiting the positive trends co-located with the positive climatolgoies and negative trends co-located with the negative climatologies (Fig. 8b). This suggests that the wavenumber-1 wave intensity during 1998–2018 weakens but the wavenumber-2 wave intensity during this period strengthens, consistent with the results in Hu et al. (2019). Similar to the trend results, anomalies in the longitudinal and vertical structure of the wavenumber-1 and -2 components of geopotential height in response to $PC2_{SST}$ (Figs. 8c,d) exhibit positive (negative) anomalies in the zonal wavenumber-1 component of geopotential height that co-locates with the negative (positive) climatologies (Fig. 8c), suggesting a weakened wavenumber-1 planetary wave in response to the North Pacific SSTAs. However, anomalies in the wavenumber-2 component of geopotential height are in-phase with its climatologies (Fig. 8d), implying a strengthened wavenumber-2 planetary wave in response to the positive Victoria mode phases.

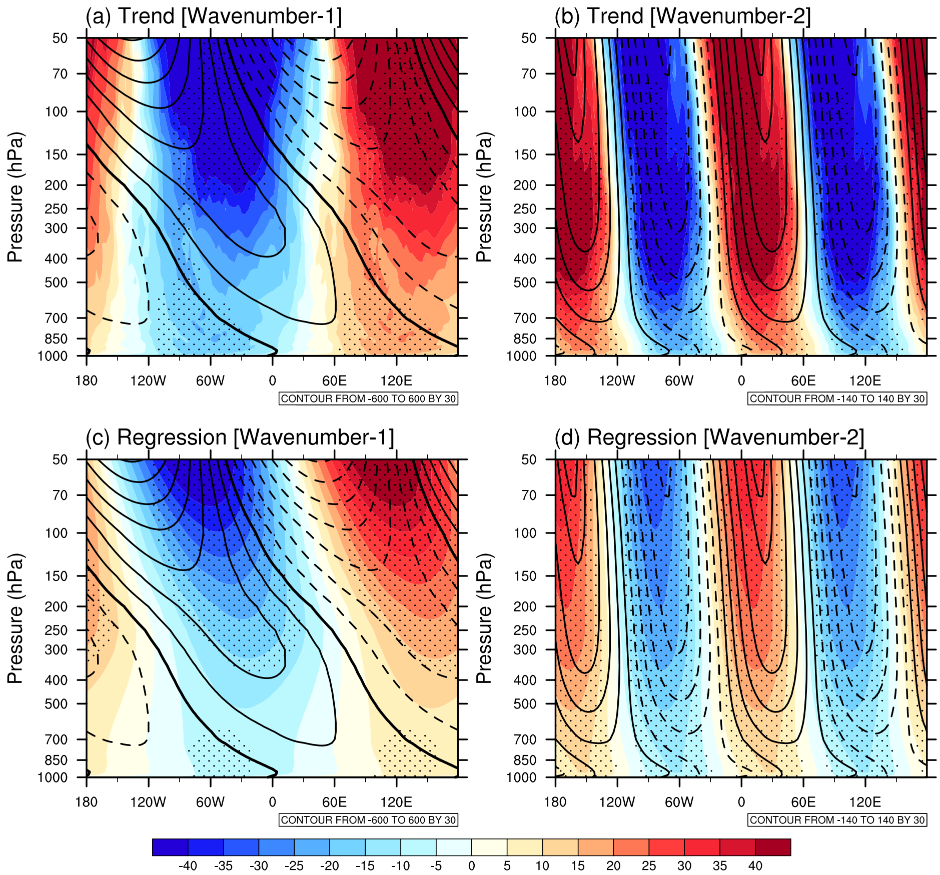

Figure 8. (a, b) Trends (shading, m decade^{-1}) in the longitudinal and vertical structure of the wavenumber-1 and -2 components of geopotential height averaged over 45°N–75°N in March during 1998–2018. (c, d) Same as (a, b), but for the geopotential height anomalies regressed on $PC2_{SST}$ in February during 1980–2018. The contours represent the climatological mean of wavenumber-1 (left panels) and -2 (right panels) components of geopotential height averaged over 45°N–75°N. The values over the stippled regions are statistically significant at the 90% confidence level.

The details of the weakened wavenumber-1 and strengthened wavenumber-2 wave intensity during 1998–2018 can be seen more clearly in Figs. 9a,b. Meanwhile, Figures 9c–d give the regressed anomalies in the wavenumber-1 and -2 components of geopotential height at 200 hPa based on $PC2_{SST}$. The out-of-phase (in-phase) between the anomalies and climatologies in the wavenumber-1 (-2) components of geopotential height in response to the North Pacific SSTAs (Fig. 8) can clearly be seen in the maps at 200 hPa (Figs. 9c–d). Above results suggest that the weakened WP and strengthened PNA patterns in response to the positive Victoria mode phases are consistent with the weakened wavenumber-1 component in the wave activity over the upper troposphere and lower stratosphere, which plays a dominant role in the weakening of the stratospheric wave flux in response to the Victoria mode. But the strengthening of the wavenumber-2 components associated with the Victoria mode counteract the weakening of wavenumber-1 to some extent.

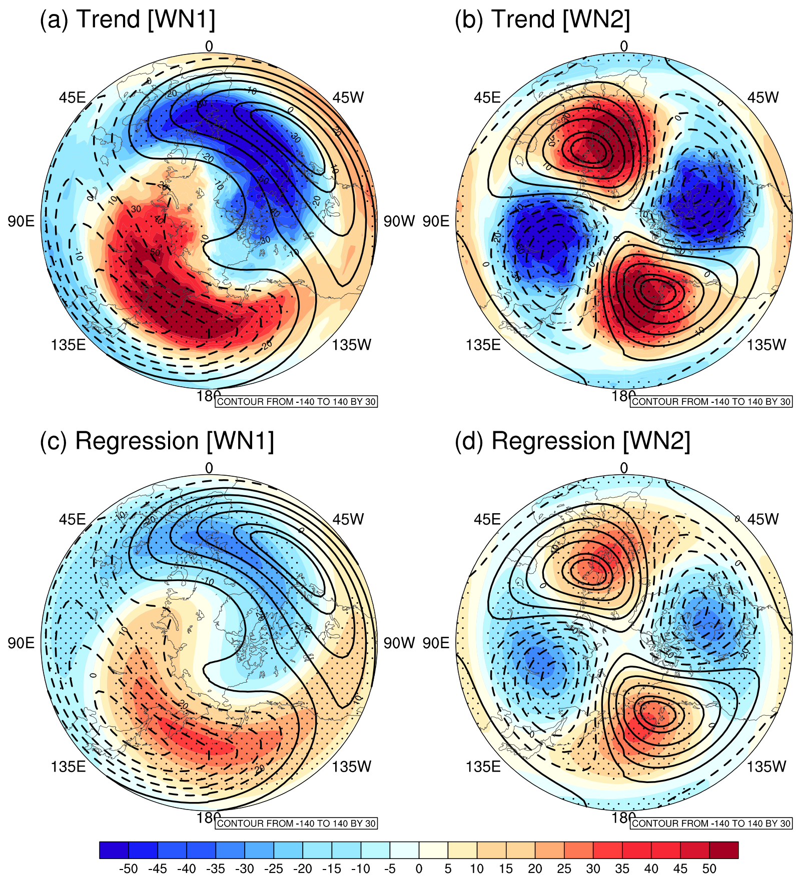

Figure 9. (a, b) Trends (shading, m decade^{-1}) in the wavenumber-1 and -2 components of geopotential height at 200 hPa in March during 1998–2018. (c, d) Same as (a, b), but for the geopotential height anomalies regressed on $PC2_{SST}$ in February during 1980–

2018. The contours represent the climatological mean of wavenumber-1 (left panels) and -2 (right panels) components of geopotential height at 200 hPa. Dotted regions represent the values statistically significant at the 90% confidence level.

The quasi-geostrophic Eliassen–Palm (EP) flux (Edmon et al., 1980) is chosen to diagnose the propagation of planetary waves. During 1998–2018, there are weakened trends in the wavenumber-1 wave propagation in the lower stratosphere (Fig. 10a) but strengthened trends in the wavenumber-2 wave propagation (Fig. 10b), which are consistent with the weakened wavenumber-1 wave intensity and strengthened wavenumber-2 wave intensity during this period (Figs. 8a–b). In response to $PC2_{SST}$, there are weakened upward planetary wavenumber-1 waves in the lower stratosphere over the Arctic region (Fig. 10c), with slightly strengthened meridional propagation at mid-latitude in the upper troposphere. However, the planetary wavenumber-2 waves in response to $PC2_{SST}$ exhibit strengthened upward propagation in the lower stratosphere with weakened equatorward propagation at mid-latitude in the upper troposphere (Fig. 10d). The weakened wavenumber-1 upward propagation and strengthened wavenumber-2 upward propagation (Fig. 10) are in accord with the weakened wavenumber-1 component but strengthened wavenumber-2 component in the wave activity over the upper troposphere and lower stratosphere shown in Fig. 8. Note that the weakened upward planetary wavenumber-1 wave propagation is accompanied with positive zonal wind anomalies over the Arctic and negative anomalies at mid-latitudes. This indicates that the subtropical westerly jet weakens in response to the positive $PC2_{SST}$ phases, which may not favor the planetary wave upward propagation according to the wave–mean flow interaction theory (Andrews et al., 1987).

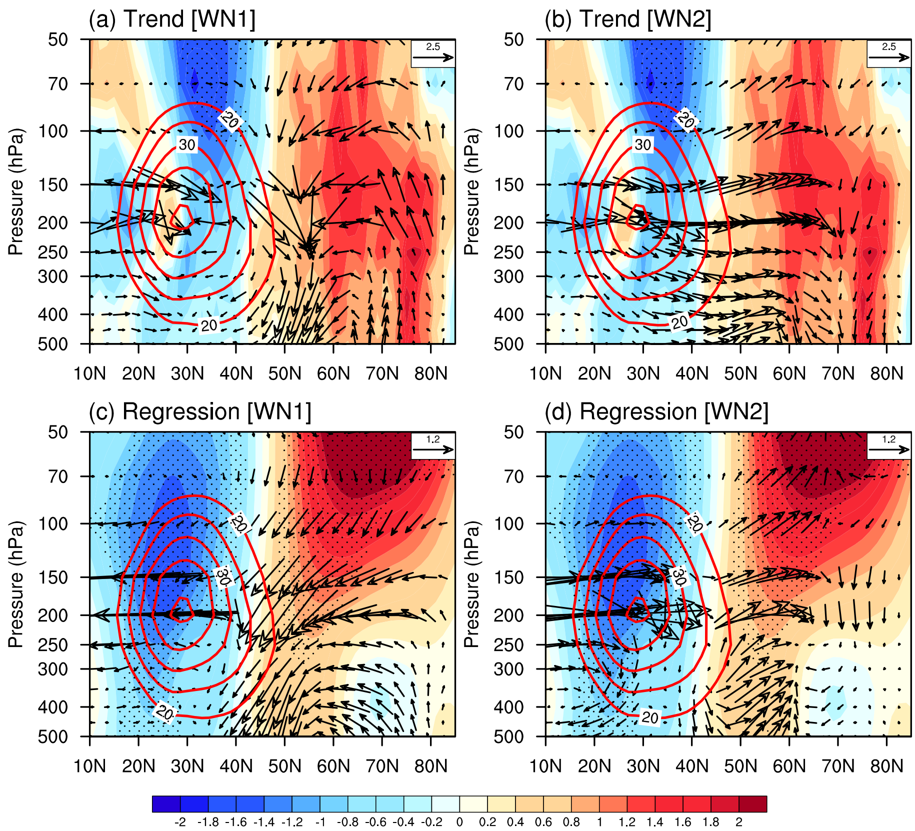

Figure 10. (a, b) Trends in the zonal winds (shading, m s^{-1} $decade^{-1}$) and (a) wavenumber-1 and (b) wavenumber-2 components of EP flux (arrows with units of 10^4 kg s^{-2} $decade^{-1}$ for vertical vectors and 10^6 kg s^{-2} $decade^{-1}$ for horizontal vectors over 50–200 hPa, and 5×10^4 kg s^{-2} $decade^{-1}$ for vertical vectors and 5×10^6 kg s^{-2} $decade^{-1}$ for horizontal vectors over 250–500 hPa, respectively) in March during 1980–2018. (c, d) Same as (a, b), but for the regressed anomalies in the zonal winds (shading, m s^{-1} $decade^{-1}$) and (c) wavenumber-1 and (d) wavenumber-2 components of EP flux (arrows with units of 10^4 kg s^{-2} for vertical vectors and 10^6 kg s^{-2} for horizontal vectors over 50–200 hPa, and 5×10^4 kg s^{-2} for vertical vectors and 5×10^6 kg s^{-2} for horizontal vectors over 250–500 hPa, respectively) in March based on $PC2_{SST}$ in February during 1980–

2018. The contours represent the climatologies of zonal winds (only values above 20 m s^{-1} are shown), respectively. Dotted regions represent the values statistically significant at the 90% confidence level.

As the BDC is closely related to the stratospheric planetary wave activity (Butchart et al., 2014 and references therein), the BDC possibly weakens in response to the positive $PC2_{SST}$ because of the weakened propagation of planetary wave in response to the SSTAs over the North Pacific. Figure 11 further shows the trends in the March velocities of BDC during 1998–2018 and their anomalies regressed on $PC2_{SST}$ in February during 1980–2018. The vertical velocity of BDC during 1998–2018 exhibits negative trends at subpolar regions but positive trends at polar regions (Fig. 11a), along with the negative trends in the meridional velocity of BDC at extratropics in the stratosphere (Fig. 11b). It seems that the extratropical downwelling in the NH after 1998 does not totally weaken, but with some regional characteristics, i.e., the BDC weakens over the Arctic but strengthens at subpolar regions, which need more investigation. Because we focused on the decreasing trends in the stratospheric ozone over the Arctic, the anomalies in the BDC velocities over the Arctic related to the North Pacific SSTAs are paid more attention to. As expected, there are weakened anomalies in the downwelling velocity over the Arctic compared to its climatology in response to the warmed North Pacific SSTAs (Fig. 11c), which implies a weakened BDC to the North Pacific SSTAs.

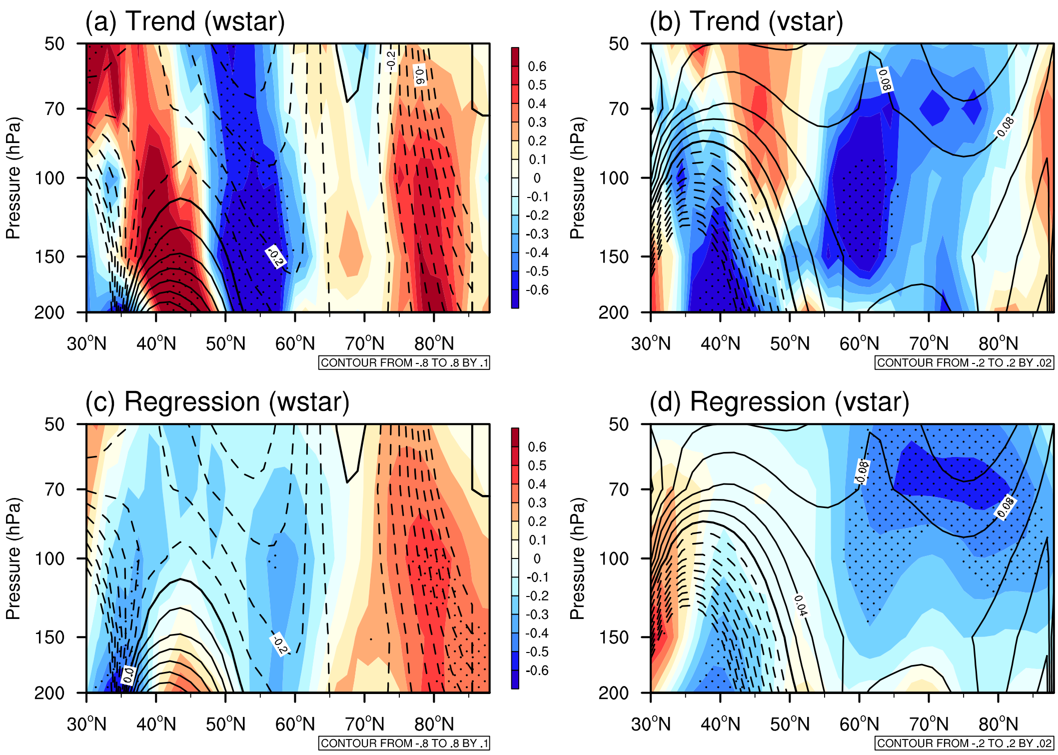

Figure 11. (a, b) Trends in the March (a) w^* (mm s^{-1} decade^{-1}) and (b) v^* (m s^{-1} decade^{-1}) during 1980–2018. (c, d) Anomalies in the March w^* (mm s^{-1}) and v^* (m s^{-1}) regressed on $PC2_{SST}$ in February during 1980–2018. The dashed and solid contours represent the negative and positive climatological mean of w^* and v^*in March, respectively. The values over the stippled regions are statistically significant at and above the 90% confidence level.

Changes in the BDC could modulate concentrations of ozone in the stratosphere (e.g., Hu et al., 2014; 2015). Anomalies in the lower-stratospheric ozone over the Arctic caused by the BDC and eddy transport can be examined according to the Transformed Eulerian-Mean formulation of the zonal-mean ozone tracer continuity equation (Garcia & Solomon, 1983) (more details in the section of 2.3). Figure 12 further shows the trends in the March ozone produced by the BDC and eddy during 1998–2018 and the associated anomalies regressed on $PC2_{SST}$ in February during 1980–2018. The ozone caused by changes in the meridional and vertical velocities of BDC during 1998–2018 exhibits positive trends at mid-latitudes, negative trends at high-latitudes (Figs. 12a,b). However, the ozone trends caused by changes in the eddy during this period are different, i.e., positive trends at high-latitudes but negative trends at mid-latitudes (Fig. 12c). These results imply that the ozone trends over the Arctic in the stratosphere are related to both the BDC and the eddy transport. Looking at Fig. 12 and Fig. 1 together, it seems that the vertical transport from BDC might play the dominant role in the decreasing trend in the ozone concentration during this period. In response to the North Pacific SSTAs, there are positive ozone anomalies caused by changes in the meridional BDC velocity (Fig. 12d) and eddy transport (Fig. 12f) in the Arctic lower stratosphere, but statistically significant negative ozone anomalies caused by the vertical transport of BDC there (Fig. 12e). These imply that the lower-stratospheric ozone anomalies over the Arctic in response to $PC2_{SST}$ are mainly caused by vertical transport of the BDC, and not by the eddy transport. However, the eddy transports in response to $PC2_{SST}$ can result in negative anomalies of lower-stratospheric ozone at mid-latitudes. The weakened BDC downwelling velocity over the Arctic (Fig. 11) may result in negative anomalies in the lower-stratospheric ozone over the Arctic via weakening the ozone transport from the ozone-rich middle stratosphere to the ozone-poor lower stratosphere (Fig. 12).

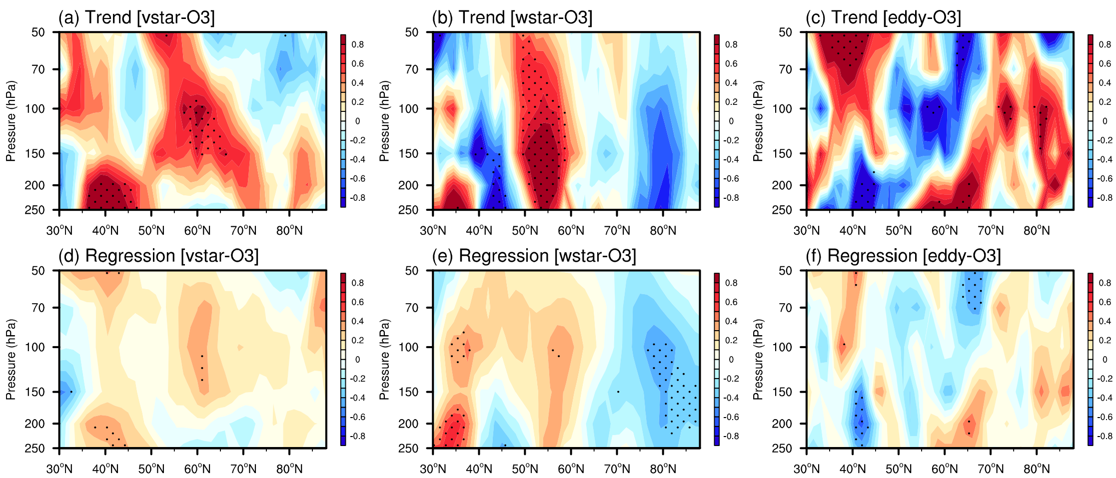

Figure 12. Trends in the March ozone (a) v^*-produced, (b) w^*-produced, and (c) eddy transported during 1980–2018. (d–f) Same as (a–c), but for the anomalies in the March ozone (d) v^*-produced, (e) w^*-produced, and (f) eddy transported regressed on $PC2_{SST}$ in February during 1980–2018. Dotted regions represent the values statistically significant at and above the 90% confidence level.

Besides changes in the BDC and eddy transport, the temperatures in the Arctic stratosphere can be also controlled by the anomalous planetary wave activity associated with the North Pacific SSTs. Figure 13 shows the trends in the temperature and zonal winds in March during 1998–2018 and their anomalies regressed on $PC2_{SST}$ in February during 1980–2018. During 1998–2018, the temperature over the Arctic exhibits negative trends (Fig. 13a) along with the positive trends in the zonal winds there (Fig. 13b), but most of these trends are insignificant. In response to the warmed North Pacific SSTAs, there are cooling anomalies in the lower-stratospheric temperature over the Arctic (Fig. 13c) and strengthened anomalies in the zonal winds (Fig. 13d). These anomalies are in accord with the decreased ozone anomalies. The stronger and more variable wave driving can affect the ozone concentrations by both ozone transport (dynamical resupply) and chemical depletion (e.g., Strahan et al., 2016), i.e., stronger (weaker) wave driving is closely associated with increased (decreased) ozone by dynamical resupply and increased (decreased) ozone by reducing (increasing) chemical loss. In addition to the ozone decrease caused by the weakened BDC in response to the Victoria mode (Figs. 11 and 12), the cooler Arctic stratosphere (Fig. 13) can increase polar stratospheric cloud occurrence, on whose surface chlorine-activating heterogeneous reactions occur, further reducing the ozone (Solomon et al., 1994; Chipperfield et al., 1999; Daniel et al., 1999). If the temperatures are low enough and active chlorine is present during boreal spring, particularly following cold winters, such as 1997 and 2011 (Chipperfield, 2015), and 2020 (Rao and Garfinkel, 2020), photochemical ozone loss may depress the temperature, which in turn enhances the chemical reactions and leads to more ozone loss.

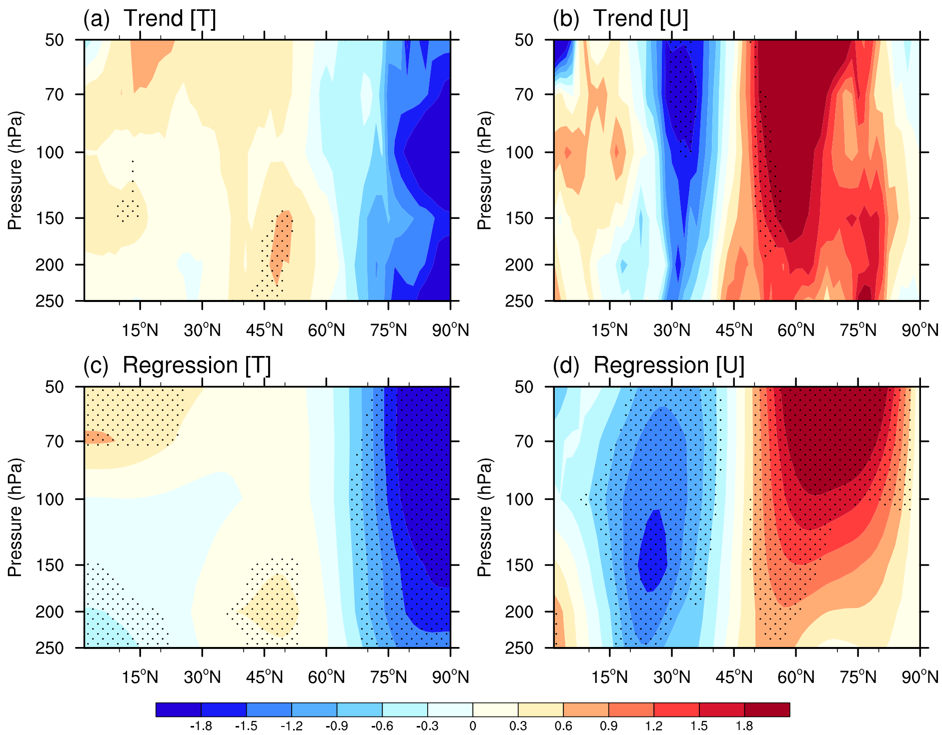

Figure 13. (a, b) Trends in (a) temperature and (b) zonal winds in March during 1980–

2018. (c, d) Anomalies in (c) temperature and (d) zonal winds in March obtained by the regression on the $PC2_{SST}$ in February during 1980–2018. Dotted regions represent the values statistically significant at the 90% confidence level.

6. Conclusions and discussion

Using meteorological reanalysis, several observational datasets and a chemical transport model, trends in the concentrations of lower-stratospheric ozone over the Arctic and its links to the SSTAs over the North Pacific are examined in this study. Our results show a decreasing trend in the concentrations of ozone in March of –0.12±0.07 ppmv decade^{-1} from MERRA2 and –0.09±0.07 ppmv decade^{-1} from TOMCAT after 1998, in the period following the turnaround in the atmospheric ODS levels.

Further analysis suggested that the North Pacific SSTAs associated with the second leading mode in February appear to have impacts on the lower-stratospheric ozone over the Arctic in March with a contribution of about 30%. Ozone concentrations decrease with the warm phases of Victoria mode-related North Pacific SSTAs, and increase with the North Pacific SSTAs associated with its cold phases. The decrease in ozone over the lower stratospheric Arctic during 1998–2018 is consistent with an increase in the PC2 of the North Pacific SSTAs. The Victoria-mode-related SSTAs tend to result in a weakened Aleutian low accompanied by a strengthening in the WP pattern and a weakening in the PNA pattern, which impede the upward propagation of wavenumber-1 waves into the subpolar lower stratosphere. In response to the Victoria mode, the BDC is weakened via weakening the wave propagation, which results in the negative anomalies in the lower-stratospheric ozone over the Arctic via weakening the ozone transport from the middle stratosphere of ozone-rich to the ozone-poor lower stratosphere. Besides these dynamical processes, the cooler and stronger Arctic stratosphere in response to the North Pacific SSTAs related to the Victoria mode may also affect the ozone concentrations through chemical depletion, which needs further investigation. It is also worth clarifying that a trend of two decades could reflect decadal variability that is likely to reverse going forward, rather than, say, an anthropogenically forced signal.

Some previous studies investigated the connections between the stratospheric Arctic vortex and North Pacific SSTs associated with Pacific decadal oscillation (PDO) (e.g., Hurwitz et al., 2012; Woo et al., 2015; Kren et al., 2016; Hu et al., 2018). These studies showed that the warming in the North Pacific associated with the positive PDO phases could result in a stronger stratospheric Arctic vortex. While some other studies investigated the potential linkage between the Victoria mode-related North Pacific SSTAs with stratosphere (e.g., Xie et al., 2017; Li et al., 2018). Li et al. (2018) revealed that the positive phases of PC2 of North Pacific SSTAs tend to result in more frequent stratospheric sudden warming (SSW) events and longer SSW duration than their negative phases. That is, the warming in the North Pacific SSTs associated with the second leading mode of North Pacific SSTAs might lead to less SSW events (Li et al., 2018), suggesting more strong stratospheric vortex events. From this view, it seems that the stratospheric polar vortex might be not sensitive to the pattern of SSTAs over the North Pacific, but to the warming somewhere over the North Pacific. But it does not mean that the warming anywhere in the North Pacific will lead to a stronger vortex, because the warming related to the PDO and Victoria mode both are not uniform all over the North Pacific Ocean. A recent study suggested that a warming over the central North Pacific could lead to a stronger stratospheric polar vortex (Hu et al., 2018). The central North Pacific is the overlapping region of the PDO and Victoria mode of North Pacific SSTAs, we infer that the stratospheric polar vortex might be more sensitive to the warming over the central North Pacific. The connections between the stratospheric ozone over the Arctic with the warming in the North Pacific over different regions are still unclear, which are worthy of further investigation.

Recall that the ozone trends in the tropics and NH midlatitudes, and the potential mechanism, are under wide debate (e.g., Ball et al. 2018, 2019; Wargan et al., 2018; Chipperfield et al., 2018b; Orbe et al., 2020). Wargan et al. (2018) provided the evidence for a dynamical origin of the observed decreased trend in the ozone in the extratropical lower stratosphere, which corroborated the results of Ball et al. (2018). Chipperfield et al. (2018b) argued that these trends resulted from natural variability. That met with a response from Ball et al. (2019) who demonstrated robustness of the trends through 2018. Orbe et al. (2020) demonstrated that the trends in ozone in the lower stratosphere in the NH midlatitudes result from trends in the residual circulation. In this paper, we link the polar ozone in the stratosphere to the BDC. Furthermore, Ball et al. (2020) suggests changes in mixing as a mechanism underpinning these trends, consistent with Wargan et al (2018), and points to an apparent inability of free-running models to reproduce the observed the lower-stratospheric ozone behavior. The latter point is also elaborated on extensively by Dietmüller et al. (2021). This present work explored the trends in the stratospheric ozone over the Arctic and uniquely linked the recent ozone depletion in the stratosphere over the Arctic to the North Pacific SSTs, which might provide another important element to the debate.

Acknowledgements

We thank Professor Martyn Chipperfield for useful comments and suggestions. We are grateful to the groups and agencies for providing the datasets used in this study, including the Merra2 (https://disc.gsfc.nasa.gov/datasets/M2IMNPASM_V5.12.4/summary?keywords= merra-2), GOZCARDS (https://disc.gsfc.nasa.gov/datasets/GozSmlpO3_V1), ERA5 (https://cds.climate.copernicus.eu/cdsapp#!/dataset/reanalysis-era5-pressure-levels-monthly-means?tab=form), SBUV (https://disc. gsfc.nasa.gov/datasets/SBUV2N09L3zm_V1), SWOOSH (http://www.esrl.noaa.gov/csd/groups/ csd8/swoosh/), MLS (https://disc.gsfc.nasa.gov/datasets), and ERSST V5 (https://www.esrl. noaa.gov/psd/data/gridded/data.noaa.ersst.v5.html). This work was supported by the National Key R&D Program of China (2019YFC1510201) and the National Natural Science Foundation of China (42175072, 41805031).

References

Andrews, D. G., Holton, J. R. & Leovy, C. B. *Middle Atmosphere Dynamics*. Academic Press Inc., 489 pp (1987).

Ball, W. T. et al. Evidence for a continuous decline in lower stratospheric ozone offsetting ozone layer recovery. *Atmos. Chem. Phys.,* **18,** 1379–1394 (2018).

Ball, W. T., Alsing, J., Staehelin, J., Davis, S. M., Froidevaux, L. & Peter, T. Stratospheric ozone trends for 1985–2018: sensitivity to recent large variability, *Atmos. Chem. Phys.,* **19:** 12731–12748 (2019).

Ball, W. T., Chiodo, G., Abalos, M., Alsing, J. & Stenke, A. Inconsistencies between chemistry–climate models and observed lower stratospheric ozone trends since 1998. *Atmos. Chem. Phys.,* **20:** 9737–9752 (2020).

Bednarz, E. M., Maycock, A. C., Abraham, N. L., Braesicke, P., Dessens, O. & Pyle, J. A. Future Arctic ozone recovery: the importance of chemistry and dynamics. *Atmos. Chem. Phys.,* **16,** 12159–12176 (2016).

Bhartia, P. K. et al. Solar Backscatter UV (SBUV) total ozone and profile algorithm. *Atmos. Meas. Tech*., **6,** 2533–2548 (2013).

Bond, N. A., Overland, J. E., Spillane, M. & Stabeno, P. Recent shifts in the state of the North Pacific. *Geophys. Res. Lett.,* **30,** 2183 (2003).

Bourassa, A. E. et al. Trends in stratospheric ozone derived from merged Odin-OSIRIS and SAGE II satellite observations. *Atmos. Chem. Phys.,* **14,** 6983–6994 (2014).

Butchart, N. The Brewer-Dobson circulation. *Rev. Geophys.,* 52: 157–184 (2014).

Calvo, N., Polvani, L. M. & Solomon, S. On the surface impact of Arctic stratospheric ozone extremes. *Environ. Res. Lett.,* **10,** 094003 (2015).

Chipperfield, M. P. & Jones, R. L. Relative influences of atmospheric chemistry and transport on Arctic ozone trends. *Nature,* **400,** 551–554 (1999).

Chipperfield, M. P. New version of the TOMCAT/SLIMCAT off-Line chemical transport model: Intercomparison of stratospheric tracer experiments. *Quart. J. Roy. Meteor. Soc.*, **132,** 1179-1203 (2006).

Chipperfield, M. P., Dhomse, S. S., Feng, W., McKenzie, R. L., Velders, G. J. M. & Pyle, J. A. Quantifying the ozone and ultraviolet benefits already achieved by the Montreal Protocol. *Nat Commun.*, **6,** 7233 (2015).

Chipperfield, M. P. et al. Quantifying the ozone and ultraviolet benefits already achieved by the Montreal Protocol. *Nat. Commun.,* **6,** 7233 (2018a).

Chipperfield, M. P. et al. On the cause of recent variations in lower stratospheric ozone. *Geophys. Res. Lett.,* **45** (2018b).

Cohen, Y. et al. Climatology and long-term evolution of ozone and carbon monoxide in the upper troposphere–lower stratosphere (UTLS) at northern midlatitudes, as seen by IAGOS from 1995 to 2013. *Atmos. Chem. Phys.*, **18**, 5415–53 (2018).

Czaja, A. & J. Marshall. Observations of atmosphere–ocean coupling in the North Atlantic. *Quart. J. Roy. Meteor. Soc.,* **127,** 1893–1916, (2001).

Dameris, M., Loyola, D. G., Nützel, M., Coldewey-Egbers, M., Lerot, C., Romahn, F. & van Roozendael, M. Record low ozone values over the Arctic in boreal spring 2020. *Atmos. Chem. Phys.,* **21,** 617–633 (2021).

Daniel, J. S., Solomon, S., Portmann, R. W. & Garcia R. R. Stratospheric ozone destruction: The importance of bromine relative to chlorine. *J. Geophys. Res. Atmos.,* **104,** 23, 871-23,880 (1999).

Davis, S. M. et al. The Stratospheric Water and Ozone Satellite Homogenized (SWOOSH) database: a long-term database for climate studies. *Earth. Syst. Sci. Data.,* **8,** 461–490 (2016).

Davis, S. M. et al. Assessment of upper tropospheric and stratospheric water vapor and ozone in reanalyses as part of S-RIP. *Atmos. Chem. Phys.,* **17,** 12743–12778, (2017).

Hu, D., Z. Guan, Y. Guo, C. Lu, D. Jin. Dynamical connection between the stratospheric Arctic vortex and sea surface temperatures in the North Atlantic. *Clim. Dyn.,* 53, 6979–6993, (2019).

Rao, J., & Garfinkel, C. I. (2020). Arctic ozone loss in March 2020 and its seasonal prediction in CFSv2: A comparative study with the 1997 and 2011 cases. *J. Geophys. Res.* 125, e2020JD033524. https://doi.org/10.1029/2020JD033524

Dee, D. P. et al. The ERA-Interim reanalysis: Configuration and performance of the data assimilation system. *Quart. J. Roy. Meteor. Soc.,* **137,** 553–597, (2011).

Dhomse, S. et al. Estimates of ozone return dates from Chemistry-Climate Model Initiative simulations. *Atmos. Chem. Phys.,* **18,** 8409–8438 (2018).

Dietmüller, S., Garny, H., Eichinger, R. & Ball, W. T. Analysis of recent lower stratospheric ozone trends in chemistry climate models. *Atmos. Chem. Phys. Discuss.,* https://doi.org/10.5194/acp-2020-947, in review, (2021).

Ding, R., Li, J., Tseng, Y. H., Sun, C. & Guo, Y. The Victoria mode in the North Pacific linking extratropical sea level pressure variations to ENSO. *J. Geophys. Res.* **120,** 27–45 (2015).

Douglass, A. R., Rood, R. B. & Stolarski, R. S. Interpretation of ozone temperature correlations: 2. Analysis of SBUV ozone data. *J. Geophys. Res.-Atmos.,* **90,** 10693–10708, (1985).

Duchon, C. Lanczos filtering in one and two dimensions. *J. Appl. Meteor.,* **18,** 1016–1022 (1979).

Dunkerton, T. On the Mean Meridional Mass Motions of the Stratosphere and Mesosphere. *J. Atmos. Sci.,* **35,** 2325–2333 (1978).

Edmon, H. J., Hoskins, B. J. & McIntyre, M. E. Eliassen-Palm cross-sections for the troposphere, *J. Atmos. Sci.*, **37**, 2600–2616 (1980).

Eyring, V. et al. Multimodel projections of stratospheric ozone in the 21st century. *J. Geophys. Res. Atmos.*, **112**, D16303 (2007).

Feng, W., Dhomse, S. S., Arosio, C., Weber, M., Burrows, J. P., Santee, M. L., & Chipperfield, M. P. Arctic ozone depletion in 2019/20: Roles of chemistry, dynamics and the Montreal Protocol. *Geophys. Res. Letts.,* **48,** e2020GL091911 (2021).

Froidevaux, L. et al. Global Ozone Chemistry And Related Datasets for the Stratosphere (GOZCARDS): methodology and sample results with a focus on HCl, H2O, and O3. *Atmos. Chem. Phys.,* **15,** 10471–10507 (2015).

Garcia, R. R. & Solomon, S. A Numerical Model of the Zonally Averaged Dynamical and Chemical Structure of the Middle Atmosphere. *J. Geophys. Res.,* **88,** 1379–1400, (1983).

García-Herrera, R., Calvo, N., Garcia, R. R. & Giorgetta, M. A. Propagation of ENSO temperature signals into the middle atmosphere: a comparison of two general circulation models and ERA-40 reanalysis data. *J. Geophys. Res.* **111,** (2006).

Garfinkel, C. I., Hurwitz, M. M. & Oman, L. D. Effect of recent sea surface temperature trends on the Arctic stratospheric vortex. *J. Geophys. Res.,* **120,** 5404–5416 (2015).

Garfinkel, C. I. & Hartmann, D. L. Different ENSO teleconnections and their effects on the stratospheric polar vortex. *J. Geophys. Res.,* **113,** D18114, (2008).

Gelaro, R. et al. The Modern-Era Retrospective Analysis for Research and Applications, Version 2 (MERRA-2). *J. Climate* (2017) **30:** 5419–5454.

Grooss, J. U. et al. On the discrepancy of HCl processing in the core of the wintertime polar vortices. *Atmos. Chem. Phys.,* **18,** 8647-8666 (2018).

Harari, O., et al. Influence of Arctic stratospheric ozone on surface climate in CCMI models. *Atmos. Chem. Phys.,* **19,** 9253–9268 (2019).

Hartmann, D. L. Some aspects of the coupling between radiation, chemistry, and dynamics in the stratosphere. *J. Geophys. Res.-Oceans,* **86,** 9631–9640, (1981).

Hersbach, H. et al. Global reanalysis: goodbye ERA-Interim, hello ERA5. ECMWF. Meteorology section of ECMWF Newsletter No. 159– Spring 2019, pp. 17-24. https://doi.org/10.21957/vf291hehd7 (2019).

Huang, B. et al. Extended Reconstructed Sea Surface Temperature, Version 5 (ERSSTv5): Upgrades, Validations, and Intercomparisons. *J. Clim.,* **30,** 8179–8205 (2017).

Hu, Y. & Tung, K. K. Possible ozone-induced long-term changes in planetary wave activity in late winter. *J. Clim.,* **16,** 3027–3038 (2003).

Hu, D., Tian, W., Xie, F., Shu, J. & Dhomse, S. Effects of meridional sea surface temperature changes on stratospheric temperature and circulation. *Adv. Atmos. Sci.*, **31**, 888–900 (2014).

Hu, D., Tian, W., Xie, F., Wang, C. & Zhang, J. Impacts of stratospheric ozone depletion and recovery on wave propagation in the boreal winter stratosphere. *J. Geophys. Res. Atmos.*, **120**, 8299–8317 (2015).

Hu, D., Guan, Z., Tian, W. & Ren, R. Recent strengthening of the stratospheric Arctic vortex response to warming in the central North Pacific. *Nat Commun.*, **9**, 1697 (2018).

Hurwitz, M. M., Newman, P. A. & Garfinkel C. I. The Arctic vortex in March 2011: a dynamical perspective. *Atmos. Chem. Phys.,* **11,** 11447-11453 (2011).

Hurwitz, M. M., Newman, P. A. & Garfinkel, C. I. On the influence of North Pacific sea surface temperature on the Arctic winter climate. *J. Geophys. Res. Atmos.*, **117**, D19 (2012).

Inness, A. et al. Exceptionally low Arctic stratospheric ozone in spring 2020 as seen in the CAMS reanalysis. *J. Geophys. Res.,* **125,** e2020JD033563 (2020).

Ivy, D. J., Solomon, S., Calvo, N. & Thompson, D. W. J. Observed connections of Arctic stratospheric ozone extremes to Northern Hemisphere surface climate. *Environ. Res. Lett.*, **12**, 024004 (2017).

Kang, S. M., Polvani, L. M., Fyfe, J. C. & Sigmond, M. Impact of polar ozone depletion on subtropical precipitation. *Science*, **332**, 951–954 (2011).

Kendall, M. G., 1975: Rank Correlation Methods. Griffin, 202 pp.

Kramarova, N. A. et al. Validation of ozone monthly zonal mean profiles obtained from the version 8.6 Solar Backscatter Ultraviolet algorithm. *Atmos. Chem. Phys.,* **13,** 6887–6905 (2013).

Kren, A. C., Marsh, D. R., Smith, A. K., & Pilewskie, P. Wintertime Northern Hemisphere response in the Stratosphere to the Pacific Decadal Oscillation using the Whole Atmosphere Community Climate Model. *J. Climate,* **29,** 1031–1049, (2016).

Lawrence, Z. D., Perlwitz, J., Butler, A. H., Manney, G. L., Newman, P. A., Lee, S. H. & Nash, E. R. The remarkably strong Arctic stratospheric polar vortex of winter 2020: Links to record breaking Arctic Oscillation and ozone loss. *J. Geophys. Res.,* **125,** e2020JD033271 (2020).

Li, Y., et al. The connection between the second leading mode of the winter North Pacific sea surface temperature anomalies and stratospheric sudden warming events. *Clim. Dyn.,* DOI 10.1007/s00382-017-3942-0. (2018).

Manney, G. L. et al. Unprecedented Arctic ozone loss in 2011. *Nature*, **478**, 469–475 (2011).

Manney, G. L. et al. Polar processing in a split vortex: Arctic ozone loss in early winter 2012/2013. *Atmos. Chem. Phys.*, **15**, 5381–403 (2015).

Manney, G.L. et al. Record-low Arctic stratospheric ozone in 2020: MLS observations of chemical processes and comparisons with previous extreme winters. *Geophys. Res. Lett.*, **47,** e2020GL089063 (2020).

Manzini, E., Giorgetta, M. A., Esch, M., Kornblueh, L. & Roeckner, E. The influence of sea surface temperatures on the northern winter stratosphere: ensemble simulations with the MAECHAM5 model. *J. Climate*, **19,** 3863–3881 (2006).

Newman, P. A., Nash, E. R. & Rosenfield, J. E. What controls the temperature of the Arctic stratosphere during the spring? *J. Geophys Res., 106,* 19999–20010 (2001).

Orbe, C., Wargan, K., Pawson, S., & Oman, L. D. Mechanisms linked to recent ozone decreases in the Northern Hemisphere lower stratosphere. *J. Geophys Res.,* **125,** e2019JD031631 (2020).

Peng, S., Robinson, W. A. & Li, S. Mechanisms for the NAO Responses to the North Atlantic SST Tripole. *J. Climate.,* **16,** 1987–2004 (2003).

Polvani, L. M., Waugh, D. W., Correa, G. J. P. & Son, S. W. Stratospheric Ozone Depletion: The Main Driver of Twentieth-Century Atmospheric Circulation Changes in the Southern Hemisphere. *J. Climate*, **24**, 795–812 (2011).

Pyper, B. J. & Peterman, R. M. Comparison of methods to account for autocorrelation in correlation analyses of fish data. *Can. J. Fish. Aquat. Sci.,* **55,** 2127–2140, (1998).

Ramaswamy, V. et al. Radiative forcing of climate. *Clim. Change*., **349** (2001).

Rao, J. & Ren R. Asymmetry and nonlinearity of the influence of ENSO on the northern winter stratosphere: 1. Observations. *J. Geophys. Res. Atmos.,* **121,** 9000–9016, (, 2016).

Rex, M. et al. Arctic ozone loss and climate change. *Geophys. Res. Lett.*, **31,** (2004).

Rodwell, M. J., Rowell, D. P. & Folland, C. K. Oceanic forcing of the wintertime North Atlantic Oscillation and European climate. *Nature,* **398,** 320–323 (1999).

Sassi, F., Kinnison, D., Boville, B. A., Garcia, R. R. & Roble, R. Effect of El Niño–Southern Oscillation on the dynamical, thermal, and chemical structure of the middle atmosphere. *J. Geophys. Res.,* **109,** D17108, (2004).

Schwartz, M., Froidevaux, L., Livesey, N., Read, W. & Fuller, R. MLS/Aura Level 3 Monthly Binned Ozone (O3) Mixing Ratio on Assorted Grids V005, Greenbelt, MD, USA, Goddard Earth Sciences Data and Information Services Center (GES DISC), Accessed: [Data Access Date], 10.5067/Aura/MLS/DATA/3546, (2021).

Sen, P. K. Estimates of the regression coefficient based on Kendall's tau. *J. Amer. Stat. Assoc.,* **63,** 1379–1389, (1968).

Solomon, S., Garcia, R. R. & Ravishankara A. R. On the role of iodine in ozoned epletion. *J. Geophys Res.,* **99,** 20,491-20,499 (1994).

Son, S. W. et al. Impact of stratospheric ozone on Southern Hemisphere circulation change: A multimodel assessment. *J. Geophys. Res. Atmos*, **115** (2010).

Son, S-W. et al. Tropospheric jet response to Antarctic ozone depletion: An update with Chemistry-Climate Model Initiative (CCMI) models. *Environ. Res Letts.,* **13,** 054024 (2018).

Steinbrecht, W. et al. An update on ozone profile trends for the period 2000 to 2016. *Atmos. Chem. Phys.*, **17**, 10675–90 (2017).

Strahan, S. E., Douglass, A. R. & Steenrod, S. D. Chemical and dynamical impacts of stratospheric sudden warmings on Arctic ozone variability. *J. Geophys. Res. Atmos.*, **121,** (2016).

Sutton, R. T., Norton, W. A. & Jewson, S. P. The North Atlantic Oscillation—What role for the ocean? *Atmos. Sci. Lett.,* **1,** 89–100 (2000).

Thompson, D. W. J. et al. Signatures of the Antarctic ozone hole in Southern Hemisphere surface climate change. *Nat.Geosci.*, **4**, 741–749 (2011).

Tilmes, S., Müller, R., Grooß, J.-U. & Russell, J. M. Ozone loss and chlorine activation in the Arctic winters 1991-2003 derived with the tracer-tracer correlations. *Atmos. Chem. Phys.*, **4**, 2181–2213 (2004).

Tummon, F. et al. Intercomparison of vertically resolved merged satellite ozone data sets: interannual variability and long-term trends. *Atmos. Chem. Phys.*, **15**, 3021–43 (2015).

Wallace, J. M. & Gutzler, D. S. Teleconnections in the geopotential height field during the Northern Hemisphere winter. *Mon. Wea. Rev.*, **109**, 784–812 (1981).

Wargan, K. et al. Recent decline in extratropical lower stratospheric ozone attributed to circulation changes. *Geophys. Res. Lett.,* **45,** 5166–5176 (2018).

Weatherhead, E. C. & Andersen, S. B. The search for signs of recovery of the ozone layer. *Nature*, **441**, 39–45 (2006).

Witze, A. Rare ozone hole opens over Arctic—and it's big. *Nature* (2020) **580:**18.

WMO. Scientific assessment of ozone depletion: 2006: *World Meteorological Organisation, Global Ozone Research and Monitoring Project–Report*, **50**, 572 (2007).

WMO. Scientific Assessment of Ozone Depletion. Global ozone research and monitoring project (Report No. 58, p. 588). Geneva, Switzerland. Geneva, Switzerland (2018).

Wohltmann, I., P. et al. Near-complete local reduction of Arctic stratospheric ozone by severe chemical loss in spring 2020. *Geophys. Res. Lett.,* **47,** e2020GL089547 (2020).

Woo, S. H., Sung, M. K., Son, S. W., & Kug, J. S. Connection between weak stratospheric vortex events and the Pacific Decadal Oscillation. *Clim. Dyns.,* **45,** 3481–3492 (2015).

Xia, Y., Hu, Y., Zhang, J., Xie, F. & Tian, W. Record Arctic Ozone Loss in Spring 2020 is Likely Caused by North Pacific Warm Sea Surface Temperature Anomalies. *Adv. Atmos. Sci.,* 1-14 (2021).

Xie, F., Li, J., Tian, W., Feng, J. & Huo, Y. The Signals of El Niño Modoki in the Tropical Tropopause Layer and Stratosphere. *Atmos. Chem. Phys.,* **12,** 5259–5273 (2012).

Xie, F., Li, J. P., Tian, W. S. & Zhang, J. K. The Relative Impacts of El Niño Modoki, Canonical El Niño, and QBO on Tropical Ozone Changes since the 1980s. *Environ. Res. Lett.,* **9,** 064020, (2014).

Xie, F. et al. Variations in North Pacific sea surface temperature caused by Arctic stratospheric ozone anomalies. *Environ. Res. Lett.,* **12,** 114023 (2017).